



Addition of formate dehydrogenase increases the production of renewable alkane from an engineered metabolic pathway

Received for publication, March 1, 2019, and in revised form, June 8, 2019. Published, Papers in Press, June 10, 2019, DOI 10.1074/jbc.RA119.008246

Juthamas Jaroensuk^{†1}, Pattarawan Intasian^{†1}, Cholpisit Kiattisewee[‡], Pobthum Munkajohnpon^{†§}, Paweenapon Chunthaboon[§], Supacha Buttranon[‡], Duangthip Trisrivirat[§],  Thanyaporn Wongnate[‡], Somchart Maenpuen[¶], Ruchanok Tinikul[§], and  Pimchai Chaiyen^{‡2}

From the [†]School of Biomolecular Science and Engineering, Vidyasirimedhi Institute of Science and Technology (VISTEC), Wangchan Valley, Rayong 21210, the [§]Department of Biochemistry and Center for Excellence in Protein and Enzyme Technology, Faculty of Science, Mahidol University, Bangkok 14000, and the [¶]Department of Biochemistry, Faculty of Science, Burapha University, Chonburi 20131, Thailand

Edited by F. Peter Guengerich

An engineered metabolic pathway consisting of reactions that convert fatty acids to aldehydes and eventually alkanes would provide a means to produce biofuels from renewable energy sources. The enzyme aldehyde-deformylating oxygenase (ADO) catalyzes the conversion of aldehydes and oxygen to alkanes and formic acid and uses oxygen and a cellular reductant such as ferredoxin (Fd) as co-substrates. In this report, we aimed to increase ADO-mediated alkane production by converting an unused by-product, formate, to a reductant that can be used by ADO. We achieved this by including the gene (*fdh*), encoding formate dehydrogenase from *Xanthobacter* sp. 91 (*XaFDH*), into a metabolic pathway expressed in *Escherichia coli*. Using this approach, we could increase bacterial alkane production, resulting in a conversion yield of ~50%, the highest yield reported to date. Measuring intracellular nicotinamide concentrations, we found that *E. coli* cells harboring *XaFDH* have a significantly higher concentration of NADH and a higher NADH/NAD⁺ ratio than *E. coli* cells lacking *XaFDH*. *In vitro* analysis disclosed that ferredoxin (flavodoxin):NADP⁺ oxidoreductase could use NADH to reduce Fd and thus facilitate ADO-mediated alkane production. As formic acid can decrease the cellular pH, the addition of formate dehydrogenase could also maintain the cellular pH in the neutral range, which is more suitable for alkane production. We conclude that this simple, dual-pronged approach of increasing NAD(P)H and removing extra formic acid is efficient for increasing the production of renewable alkanes via synthetic biology-based approaches.

Fossil-derived hydrocarbons in the forms of natural gas and petroleum have been a major source of world energy and have served as material building blocks for decades. However, the shortage of fossil fuels and the tremendous contribution fossil fuel use has on global CO₂ emission is becoming a significant problem (1). The emergence of alternative energy sources has thus become vital to modern energy consumption. One such source is bioenergy, which now accounts for up to a 10% share of global energy consumption (2). Although various alternative energy sources such as solar, wind, and hydro power have shown promise in providing electricity and transportation for urban usage, the demands of hydrocarbon usage, especially that for alkanes for use in long-distance transportation in developing countries, household cooking, and as precursors for material synthesis still remain indispensable (3). Even though there are several methods available for biofuel production, the efficiency of bioenergy production is hardly sufficient for realistic energy demands in many countries, including the United States (4). Therefore, a sustainable method for the production of alkanes from alternative and renewable resources such as from bio-based products is very important for the security and sustainability of world energy and materials (5, 6).

Synthetic biology approaches have contributed to the construction of a metabolic pathway for the production of alkanes from renewable sources such as from fatty acids and carbohydrates. This method is a green, clean, and sustainable technology for supplying energy and materials for the future (7, 8). Particularly, the pathway targeting the conversion of fatty acids to alkanes provides a means to recycle waste containing fatty acids or triglycerides, such as those derived from oil production industries. In Southeast Asia, the main source of fatty acid or triglyceride waste is derived from palm oil mill effluent (waste from palm oil production) (9). The technology to convert fatty acid to alkane will contribute significantly to the development of a circular economy that focuses on the recycling and conversion of waste into useful materials.

Artificial cascade enzymatic reactions to generate alkanes in microbes can be achieved using the reactions of carboxylic acid

This work was supported by Thailand Research Fund Grants RTA5980001 (to P. Chaiyen), MRG6180151 (to R. T.), MRG6080234 (to T. W.), and MRG5980001 (to S. M.) and a grant from Vidyasirimedhi Institute of Science and Technology (VISTEC) (to J. J., P. I., C. K., S. B., T. W., and P. Chaiyen). Patent Application No. TH1801003340 (alkane production using the engineered metabolic pathway) was filed to the Department of Intellectual Property, Thailand.

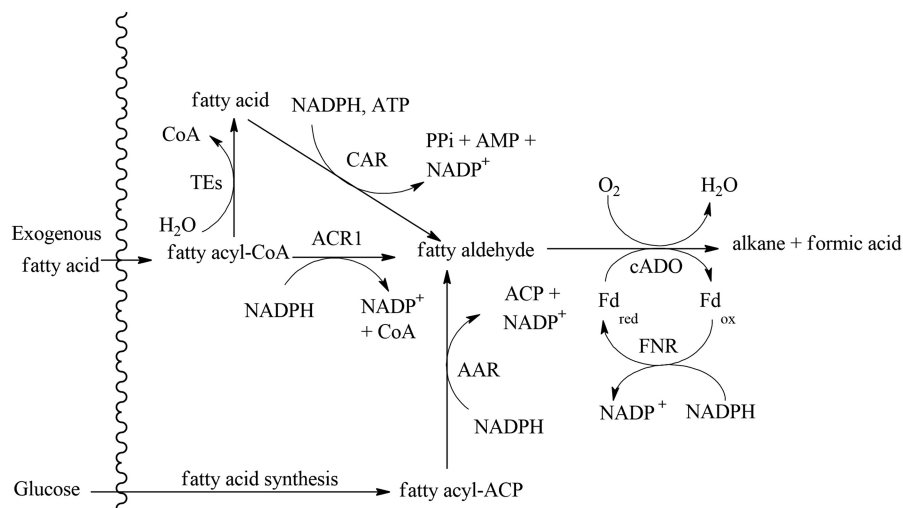
The nucleotide sequence(s) reported in this paper has been submitted to the DDBJ/GenBank™/EBI Data Bank with accession number(s) MK492106.

This article contains Figs. S1–S5 and supporting Ref. 1.

¹ Both authors contributed equally to this work.

² To whom correspondence should be addressed. E-mail: pimchai.chaiyen@vistec.ac.th.

This is an open access article under the CC BY license.



SCHEME 1. Engineered metabolic pathways for bioproduction of alkanes in bacteria as reported previously (10–16). The overall strategy for conversion of exogenous fatty acid and glucose to alkane is shown. Abbreviations used are: CoA, coenzyme A; TEs, thioesterases; ACP, acyl carrier protein; Fd_{red} , reduced ferredoxin; Fd_{ox} , oxidized ferredoxin.

Table 1
Engineering of the metabolic pathway of bio-alkane synthesis

Metabolic pathway	Host	Product	Yield	Ref.
TE/CAR/Sfp/ADO	<i>E. coli</i>	Alkane (C11 and C13)	~0.01	10
TE/ACR/CER	<i>E. coli</i>	Alkene (C15 and C17)	~2.8	11
Type II, FAS/TE/CAR/Sfp/ADO/Fd/FNR/KatE	<i>E. coli</i>	Alkane (C9, C12, C13, and C14)	~0.7	14
Type I, FAS/AAR/ADO/KatE	<i>E. coli</i>	Alkane (C15 and C17)	~0.16	12
AtoB/Hbd/Crt/Ter/TE/CAR/Sfp/ADO/Fd	<i>E. coli</i>	Alkane (C3)	~0.06	15
FabH2/AAR/ADO	<i>E. coli</i>	Alkane (C13–C17)	~8	13
TE/CAR/Sfp/ADO/Fd/FNR	<i>E. coli</i>	Alkene (C17)	~35	16
ACR1/ADO/Fd/FNR/ χ aFDH	<i>E. coli</i>	Alkane (C3–C7)	~50	This study

reductase (CAR),³ fatty acyl-CoA reductase (ACR1), or an acyl-ACP reductase to generate aldehydes from fatty acids, followed by the reaction of aldehyde-deformylating oxygenase (ADO) to generate alkane from aldehyde (Scheme 1) (10–16). This pathway allows host bacteria possessing the genes encoding these enzymes to convert fatty acids to alkanes. Previously, when glucose was used as the starting substrate for cells, the conversion yield of alkane from glucose was quite low, ~0.01–2.8% (Table 1) (10–16), due to the low flux of fatty acid generated from glucose. With the inclusion of genes encoding fatty acid and fatty acyl-CoA esterase/reductase enzymes, the efficiency of fatty acid conversion to alkanes by the engineered pathway was increased significantly (13). In the most recent report, the pathway that can convert fatty acids to alkanes as described in Scheme 1 could achieve an alkane production yield from fatty acid of ~35% (16).

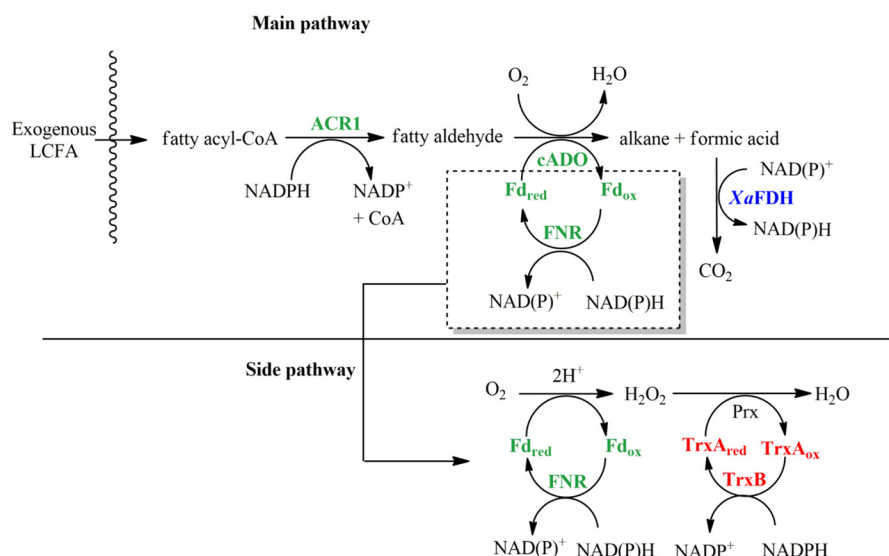
A major bottleneck of the pathway in Scheme 1 for production of alkanes is at the last enzymatic step of ADO to synthesize alkane. ADO is a slow enzyme with a low k_{cat} value. The k_{cat} of ADOs from cyanobacteria was reported to be in the range of

~0.1 min⁻¹ to 1 min⁻¹ (17–21). Under conditions in which the substrate solubility is not optimized or the availability of a reductant to activate the Fe/Fe cofactor is limited, the activity of ADO can be much lower than the reported values (17). One catalytic turnover of ADO theoretically requires four electrons in the form of reduced ferredoxin (Fd) to produce one alkane (using 2 eq of NADPH through reduction of Fd via ferredoxin (flavodoxin):NADP⁺ oxidoreductase (FNR) (14, 19, 22–24)) (Scheme 1). However, previous experiments have shown that more than 2 eq of NADPH were consumed per production of one alkane molecule because electrons in the ADO system also leaked into the pathway of oxygen reduction, leading to the formation of a hydrogen peroxide (H₂O₂) side product. H₂O₂ can inhibit the activity of ADO (14, 19), and it has been shown that the inhibitory effect of H₂O₂ on ADO activity could be alleviated in the *in vitro* assays using purified catalase (KatE) and ADO or a fusion KatE–ADO enzyme (19). However, there is no significant improvement in terms of alkane production *in vivo* (12, 14, 19).

To construct a more efficient metabolic pathway to catalyze the conversion of fatty acid to alkane as part of our effort to turn fatty acid waste into renewable alkane in the future, we used enzymology principles to address the improvement of alkane production by ADO. As 1 eq of formate is generated per 1 molecule of alkane produced (25), we aimed to capitalize on the formate as a source of a reducing equivalent to generate

³ The abbreviations used are: CAR, carboxylic acid reductase; ADO, aldehyde deformylating oxygenase; ACR1, fatty acyl-CoA reductase; EFI-EST, Enzyme Function Initiation–Enzyme Similarity Tool; Fd, ferredoxin; FDH, formate dehydrogenase; FNR, ferredoxin (flavodoxin):NADP⁺ oxidoreductase; TrxA, thioredoxin; TrxB, thioredoxin reductase; ROS, reactive oxygen species; PMSF, phenylmethylsulfonyl fluoride; IPTG, isopropyl 1-thio- β -D-galactopyranoside; LCFA, long chain fatty acid.

Metabolically-engineered pathway for alkane production



SCHEME 2. Basic metabolic pathway for production of alkanes and the refined metabolic pathway with auxiliary systems to enhance alkane production from exogenous LCFA used in this report. Enzymes and proteins associated with alkane production, formic acid elimination, and ROS detoxification are shown in *green, blue, and red*, respectively. Auxiliary systems added include formate dehydrogenase to eliminate the formic acid by-product in the main pathway and an ROS-detoxifying system to eliminate H_2O_2 in the side pathway. Abbreviation used are: CoA, coenzyme A; Fd_{red} , reduced ferredoxin; Fd_{ox} , oxidized ferredoxin; XaFDH , *Xanthobacter* formate dehydrogenase; TrxA_{ox} , oxidized thioredoxin; TrxA_{red} , reduced thioredoxin; Prx , peroxiredoxin; TrxB , thioredoxin reductase.

NAD(P)H through the reaction of formate dehydrogenase (FDH) (Scheme 2). The reaction of FDH was utilized for two purposes: the first was to produce more NAD(P)H, and the second was to remove a high concentration of formic acid. We hypothesized that a high concentration of formic acid might inhibit the reaction of ADO by ways of decreasing the overall pH of the system as well as by potentially acting as an inhibitor (product inhibition) to the system.

In this study, we constructed an engineered metabolic pathway to convert fatty acid to alkane using genes encoding for ACR1 from *Acinetobacter baumannii* and ADO from *Prochlorococcus marinus* MIT9313. Bioinformatic analysis using the Enzyme Function Initiation–Enzyme Similarity Tool (EFI–EST) option C (26) was used to find a novel FDH candidate that can use NADP^+ and NAD^+ as substrates for the production of NADPH. Results obtained from these bioinformatic analyses showed that FDH from *Xanthobacter* sp. 91 (XaFDH) is a novel FDH that has never been characterized and could be a good candidate to be used for improvement of alkane production because it can generate both NADPH and NADH from formate oxidation. Therefore, we constructed the alkane production pathway to include genes encoding auxiliary enzymes that might improve the enzymatic reaction of ADO, including XaFDH and reactive oxygen species (ROS) detoxifying enzymes thioredoxin (TrxA) and thioredoxin reductase (TrxB) from *Pseudomonas aeruginosa* PAO1. The results clearly showed that XaFDH could clearly increase the production yield of alkane to reach a conversion yield of 50%, the best yield to date for alkane production by whole-cell bioconversion.

Results

Rationale and concept of metabolic pathway construction for the biosynthesis of alkane from exogenous fatty acid

The metabolic pathway designed here (Scheme 2) aimed to use exogenous long-chain fatty acids (LCFA) as substrates to

produce long-chain hydrocarbons. In this pathway, two enzymatic steps are involved in the conversion of exogenous fatty acids to alkanes. As the first step of fatty acid uptake utilizes an endogenous long-chain fatty outer membrane transporter enzyme to attach CoA to fatty acid (27), the first enzyme that we needed to include in the engineered pathway was ACR1 (encoded by the *acr1* gene), which can convert fatty acyl-CoA to fatty aldehyde. We chose the enzyme from *A. baumannii*, which was isolated from Thai soil (28). The gene encoding for this enzyme (MK492106) was identified, cloned, and used in this study. The sequence of this enzyme shares 84% identity with ACR1 from *Acinetobacter calcoaceticus* (Fig. S1). We chose ACR1 from *Acinetobacter* sp. because it was reported that unlike ACR1 from other sources, ACR1 from *A. calcoaceticus* does not catalyze the further reduction of fatty aldehyde to fatty alcohol (29, 30). In addition, the enzyme can use a wide range of substrates such as fatty acyl-CoA containing 14–22 carbons.

At the second step, fatty aldehyde is further converted to alkane using the enzyme ADO from *P. marinus* MIT9313. The reaction of ADO (Scheme 1) requires reduced Fd, regenerated by FNR, as a co-substrate in addition to oxygen to convert aldehyde to alkane (14, 15). ADO from *P. marinus* MIT9313 was chosen for our pathway because it is one of the most characterized ADOs to date. Its known catalytic properties allow more effective usage in metabolic engineering work.

As shown in Fig. 1 for the system demonstration, we were able to produce tridecane from exogenous tetradecanoic acid in *Escherichia coli* harboring the genes for the enzymes in the basic pathway of alkane biosynthesis (Fig. 2). The constructed system was able to produce tridecane from tetradecanoic acid with ~35% yield (~300 μM tridecane from 850 μM supplied tetradecanoic acid) after 10 h of bioconversion (Fig. 1). This verified the ability to create a basic metabolically-engineered pathway for converting fatty acids to alkanes and demonstrated

that the engineered cells can use exogenous fatty acid as a substrate. Control cells in which the engineered pathway was absent did not show any production of an alkane product.

Identification, cloning, expression, and biochemical characterizations of a novel FDH suitable for increasing alkane production

Because the basic engineered metabolic pathway can produce alkanes from fatty acids with $\sim 35\%$ yield, we tried to increase the yield of alkane production by increasing the reducing power of the system using FDH to generate NAD(P)H from formate, a by-product from the reaction of ADO (Scheme 2). The purpose of this reaction is to recycle the reducing power from the formate by-product to increase the level of NAD(P)H inside the cell. NAD(P)H generated from FDH can further reduce Fd to generate reduced Fd that is a co-substrate required for the reaction of ADO. As mentioned previously in the Introduction, the rate-limiting step of the overall metabolic path is at the ADO reaction. The effort to continuously supply reduced Fd should, in principle, increase the amount of alkane product. Addition of FDH as an auxiliary redox reaction for the ADO reaction also gives another advantage in that it also removes excess formate within the cell. High concentrations of formate or formic acid can decrease the overall cellular pH of the system (see later in Fig. 7). In principle, high concentrations of accumulated product do not promote the forward reaction of ADO because the by-product formate may cause product inhibition and does not enhance the thermodynamic driving force of the forward reaction. Therefore, we identified a novel NAD(P)H-dependent FDH based on bioinformatic analysis to obtain the enzyme that can utilize formate and is suitable to be used in the metabolically-engineered pathway.

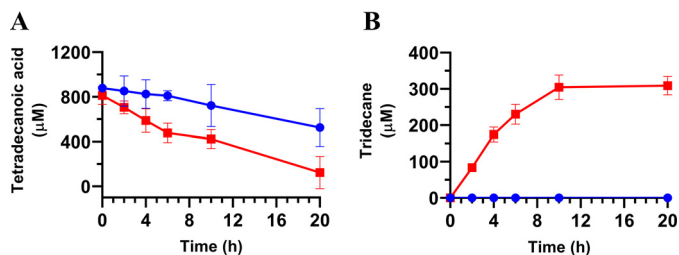


Figure 1. Production of alkane from fatty acid by the engineered cells. A, consumption of tetradecanoic acid by *E. coli*. B, tridecane production by native *E. coli* BL21 (DE3) cells is shown as blue circles, and engineered *E. coli* BL21 (DE3) cells harboring the basic pathway for alkane synthesis are shown as red squares. All data are the mean \pm S.D. ($n = 3$).

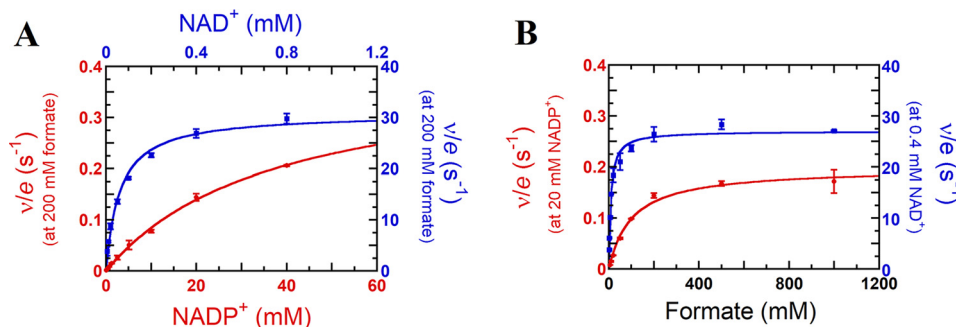


Figure 2. Steady-state kinetics of *XaFDH* reaction in 50 mM sodium phosphate buffer, pH 7.0. A, direct plots of initial rates of *XaFDH* reaction versus NAD⁺ and NADP⁺ concentrations at 200 mM sodium formate. B, direct plots of initial rates of *XaFDH* reaction versus sodium formate concentrations at 400 μM NAD⁺ and 20 mM NADP⁺. All experiments were done in triplicate, and data represent the mean \pm S.D.

Putative genes encoding for NAD(P)H-dependent FDH were identified by NCBI blastp search and were clustered by EFI-EST (26) based on the sequence similarity to the known *Pseudomonas* sp. 101 NAD(P)H-dependent FDH that is widely used in various applications (31). Two putative *fdh* genes from *Cupriavidus necator* (*Cufdh*, UniprotKB: F8GT52) and *Xanthobacter* sp. 91 (*Xafdhd*, GenBank™ ID: WP_029558741.1) were chosen for performing gene expression and activity assays as they are both in the same cluster (Fig. S2) as well-characterized NAD(P)H-dependent FDH in *Burkholderia stabilis* 15516 (32) and *Pseudomonas* sp. 101 (33), respectively.

Results from overexpression of the two selected *fdh* genes indicated that only FDH from *Xanthobacter* sp. 91 could be overexpressed in a soluble form, whereas the gene product from *C. necator* was found in inclusion bodies upon overexpression (Fig. S3A). The FDH from *Xanthobacter* sp. 91 (*XaFDH*) was successfully expressed in *E. coli* BL21 (DE3) and purified to homogeneity (see “Experimental procedures” and Fig. S3B). As *Xanthobacter* is regularly found in wastewater treatment plants from pharmaceutical and domestic effluents, we expected that *XaFDH* should be a robust enzyme suitable for future applications.

Steady-state kinetic analysis of *XaFDH* was carried out to measure K_m and k_{cat} values (see “Experimental procedures”) for the reaction using NADP⁺ and that using NAD⁺ as electron acceptors. Results (Fig. 2, A and B) indicate that *XaFDH* prefers to use NAD⁺ as an electron acceptor more than NADP⁺ because the enzyme had much lower K_m and higher k_{cat} values when NAD⁺ was used as a substrate (Fig. 2A and Table 2). The K_m values of NADP⁺ and formate for *XaFDH* were 37 ± 4 and 100 ± 13 mM, respectively, and the k_{cat} was 0.4 ± 0.02 s⁻¹. These kinetic parameters were significantly different from those with NAD⁺, which indicated the K_m values of NAD⁺ and formate for *XaFDH* as 0.060 ± 0.01 and 9 ± 1 mM, respectively, and a k_{cat} of 30 ± 1 s⁻¹. The preference of *XaFDH* for NAD⁺ as the electron acceptor over NADP⁺ was also found in other bacterial FDH, e.g. those from *Moraxella* sp. strain C-1 (34) and *Mycobacterium vaccae* N10 (35) but not from *Burkholderia* (32) and *Lactobacillus* (36), in which NADP⁺ is more preferred than NAD⁺.

Several properties of *XaFDH* were further characterized, including the enzyme thermostability, pH, and organic solvent tolerance. Results from a ThermoFluor assay revealed that *XaFDH* has a T_m of 54 °C, which is comparable with the value

Metabolically-engineered pathway for alkane production

determined for FDH from *Pseudomonas* sp. 101 (58 °C). The optimum temperature based on activity assays of *Xa*FDH also was found to be between 40 and 50 °C (Fig. 3A). We then investigated the stability of purified *Xa*FDH at 40 and 45 °C, and the results showed that *Xa*FDH activity remained the same for about 400 min of incubation (Fig. 3B). After 24 h of incubation at 40 and 45 °C, *Xa*FDH activity slightly dropped but was still retained at 70–80% of the original activity (data not shown). The data suggest that *Xa*FDH is thermostable and suitable for

catalyzing the utilization of intracellular formate. Interestingly, activity assays of *Xa*FDH at different pH values indicated that the enzyme was more active under acidic pH (Fig. 3C). The activity was increased to 5.8 ± 0.2 units/mg at pH 5.8, which was 1.5-fold higher than the activity measured at pH 8.0 (4.10 ± 0.05 units/mg). The acid preference of *Xa*FDH is advantageous for its use in engineered metabolic pathways for whole-cell biocatalysts, as our engineered metabolic pathway that generates alkanes can also increase the intracellular acidity (results shown below). The *Xa*FDH identified here is distinctive from most of the reported FDHs that show less activity under acidic conditions (37, 38). *Xa*FDH is also tolerant to organic solvent (which is required when alkane is produced from the cells) because the relative activity stayed the same as the original activity (data not shown) after incubating in 50% v/v hexane in aqueous solution for 1 h. Altogether, the *Xa*FDH identified here has enzymatic properties suitable for metabolic engineered pathways that require high temperatures, low pH values, and organic solvent.

Table 2

Kinetic parameters of *Xa*FDH using NAD⁺, NADP⁺, and formate as substrates

Kinetic parameters	<i>Xa</i> FDH
NADP⁺ and formate as substrates	
k_{cat} (s ⁻¹)	0.40 ± 0.02
K_m (mM)	
NADP ⁺	37 ± 4 ^a
Formate	100 ± 13 ^b
k_{cat}/K_m (mM ⁻¹ s ⁻¹) for NADP ⁺	0.011 ± 0.001
k_{cat}/K_m (mM ⁻¹ s ⁻¹) for formate	0.0019 ± 0.0002
NAD⁺ and formate as substrates	
k_{cat} (s ⁻¹)	31 ± 1
K_m (mM)	
NAD ⁺	0.06 ± 0.01 ^c
Formate	9 ± 1 ^d
k_{cat}/K_m (mM ⁻¹ s ⁻¹) for NAD ⁺	479 ± 30
k_{cat}/K_m (mM ⁻¹ s ⁻¹) for formate	3.0 ± 0.2

^a Data were obtained from experiments varying NADP⁺ concentrations of 0.05–40 mM at a fixed concentration of 200 mM formate.

^b Data were obtained from experiments varying formate concentrations of 5–1000 mM at a fixed concentration of 20 mM NADP⁺.

^c Data were obtained from experiments varying NAD⁺ concentrations of 0.005–0.800 mM at a fixed concentration of 200 mM formate.

^d Data were obtained from experiments varying formate concentrations of 5–1,000 mM at a fixed concentration of 0.4 mM NAD⁺. Steady-state kinetics parameters for *Xa*FDH were determined by monitoring the production of NADH and NADPH in 50 mM phosphate buffer at pH 7.0 at 25 °C.

Metabolic pathway engineering for improving alkane production

To prove our hypothesis that the addition of *Xa*FDH into an engineered metabolic pathway can improve the yield of alkane production, we constructed a new metabolic pathway (see “Experimental procedures”) to include the *fdh* gene into the basic alkane production pathway (Scheme 2). Former reports have indicated that H₂O₂ can be generated as an uncoupling side product from the reaction of ADO with oxygen and that it also inhibits the ADO reaction (12, 14, 19, 22). Thus, we also constructed other pathways that included two additional auxiliary proteins, which act to detoxify ROS in addition to the

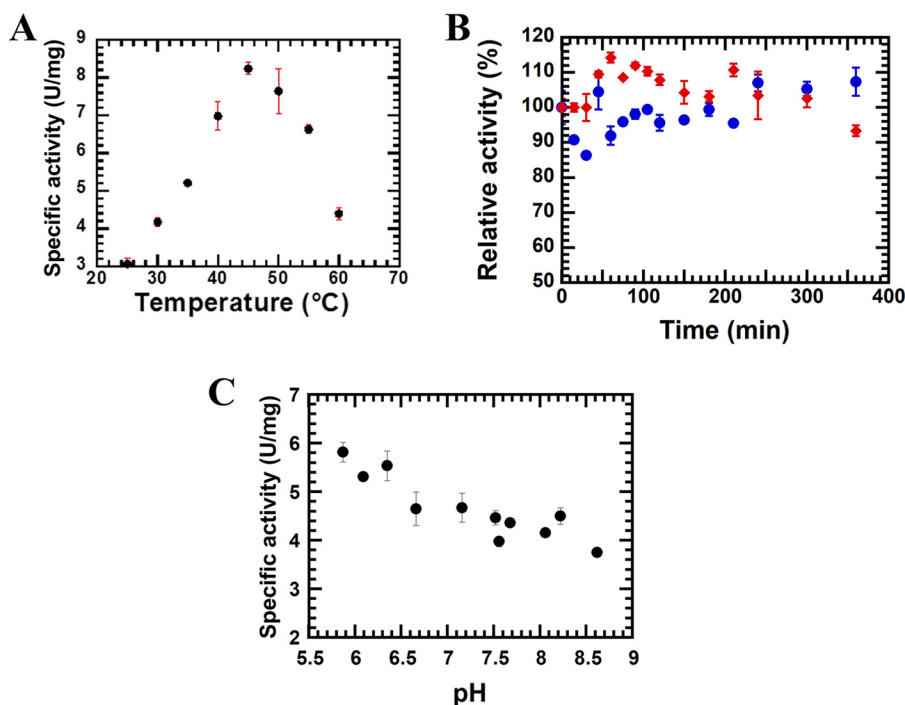
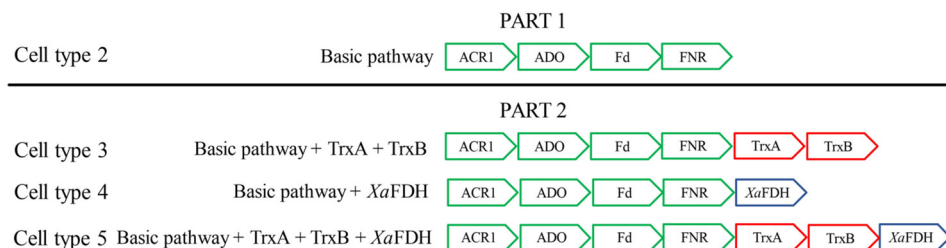


Figure 3. Effect of temperature and pH on *Xa*FDH activity. A, specific activity profiles at various temperatures (25–60 °C) indicate that the optimum temperature for the *Xa*FDH reaction was at 45 °C. B, thermostability of *Xa*FDH at 40 °C (blue circles) and 45 °C (red diamonds) was investigated by incubating the enzyme at each temperature and assayed. The data indicate that at 40 °C, *Xa*FDH could retain its original activity up to 400 min and at 45 °C up to 300 min. Activities at both temperatures were at around 80% after 24 h of incubation (data not shown). C, pH-activity profile of *Xa*FDH showed that *Xa*FDH activity decreased upon pH increases. All reactions presented herein were performed in triplicate and represented as the mean ± S.D.



SCHEME 3. Plasmids design used in this report to construct alkane synthesis pathways in *E. coli*. Part 1 is the basic metabolic pathway previously reported for bioproduction of alkane, which consists of ACR1, ADO, Fd, and FNR (cell type 2). Part 2 is the metabolic pathway for improving alkane production. The alkane-improving pathway included ROS-detoxifying enzymes (TrxA/TrxB) (cell type 3), NAD(P)H-regenerating enzyme (*XaFDH*) (cell type 4), and a combination of ROS-detoxifying enzymes (TrxA/TrxB) and NAD(P)H-regenerating enzyme (cell type 5). Abbreviations used are: ACR1, fatty acyl-CoA reductase (*A. baumannii*, Gene ID: MK492106); ADO, aldehyde-deformylating oxygenase (*P. marinus* MIT9313, Gene ID: PMT_1231); Fd, ferredoxin (*Synechocystis* sp. PCC 6803, Gene ID: ssI0020); FNR, ferredoxin (flavodoxin): NADP⁺ oxidoreductase (*E. coli*, Gene ID: b3924); *XaFDH*, *Xanthobacter* formate dehydrogenase (*Xanthobacter* sp. 91, Gene ID: WP_029558741.1); Trx, thioredoxin (*P. aeruginosa* PAO1, Gene ID: PA5240); TrxB, thioredoxin reductase (*P. aeruginosa* PAO1, Gene ID: PA2616).

added *fdh* (“Experimental procedures”). All constructed metabolic pathways are summarized in Scheme 3.

Four types of cells harboring plasmids encoding the different pathways shown in Scheme 3 were grown in Terrific Broth (TB) for 2 h. After the cell culture reached an OD₆₀₀ of 0.6, these gene sets were overexpressed by induction with 1 mM IPTG. After 6 h of protein overexpression at 25 °C, cells were harvested by centrifugation at 8000 × *g* for 10 min and were used for the bioconversion of tetradecanoic acid to tridecane. Approximately 0.85 mM tetradecanoic acid was used as the starting precursor of tridecane synthesis. The whole-cell bioconversion assay was set up in a closed vessel containing 21% O₂ (air saturation). The concentrations of tridecane and tetradecanoic acid were monitored for 0, 2, 4, 6, 10, and 20 h using a GC-MS–based method (see “Experimental procedures”).

Results as shown in Fig. 4A clearly indicate that alkane production was improved significantly in the metabolic pathway that contained *XaFDH*. The alkane production yield was improved from 35 to 50% (~426 μM) in the *E. coli* strain harboring *XaFDH* (cell types 4 and 5). These data indicate that the addition of *XaFDH* can improve alkane production as we hypothesized. Tridecane production in the *E. coli* strains expressing TrxA/TrxB (cell type 3) showed no improvement compared with the *E. coli* strain harboring the basic pathway (cell type 2), with both strains producing the same amount of tridecane (~300 μM) (Fig. 4B). The co-overexpression of TrxA/TrxB and *XaFDH* (cell type 5) did not show any improvement in alkane synthesis compared with the addition of *XaFDH* alone (cell type 4). The yield in cell type 5 generated a slightly less yield of alkane (~5%) compared with cell type 4 (Fig. 4B).

The results clearly indicate that only the *fdh* gene is required for the improvement of alkane production. The addition of ROS scavenging enzymes, TrxA and TrxB, did not improve the yield of tridecane synthesis as shown in Fig. 4A (cell types 3 and 5).

Measurement of related metabolites to identify factors underlying the improvement seen for the *XaFDH*-added metabolic pathway

As the results in Fig. 4A indicated, cells harboring the metabolically-engineered pathway with added *XaFDH* clearly showed an improved alkane production yield. Further studies were performed to identify the factors underlying the observed improvement of alkane production. Possible explana-

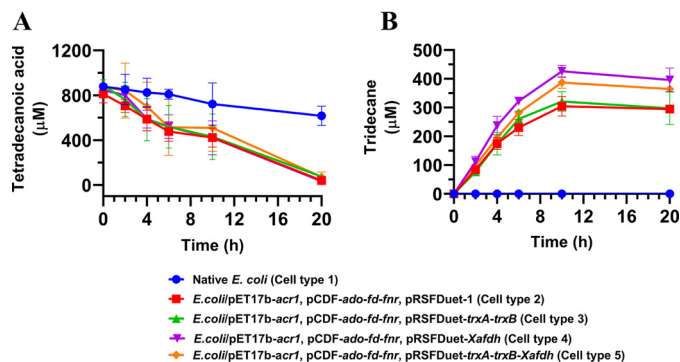


Figure 4. Improvement of alkane production by auxiliary systems. A, consumption of tetradecanoic acid by *E. coli*. B, tridecane production by native *E. coli* BL21 (DE3) cells (cell type 1) are shown as blue circles; engineered *E. coli* BL21 (DE3) cells harboring the basic pathway for alkane synthesis (cell type 2) are shown as red squares; engineered *E. coli* BL21 (DE3) cells harboring the basic pathway for alkane synthesis with ROS-detoxifying enzymes (TrxA/TrxB) (cell type 3) are shown as green triangles; engineered *E. coli* BL21 (DE3) cells harboring the basic pathway for alkane synthesis with NADH-regenerating enzyme (*XaFDH*) (cell type 4) are shown as purple triangles; and engineered *E. coli* BL21 (DE3) cells harboring the basic pathway for alkane synthesis with combined ROS-detoxifying enzymes (TrxA/TrxB) and NADH-regenerating enzyme (cell type 5) are shown as orange diamonds. All measurements were done in triplicate, and the data represent the mean ± S.D. (*n* = 3).

tions for the improvement in alkane yield include: (i) *XaFDH* increases the cellular level of NADPH/NADH that can be used to reduce Fd to generate more co-substrate for the ADO reaction; (ii) high concentrations of formate inhibit the reaction of ADO; and (iii) high concentrations of formate cause a pH drop that affects the ADO reaction. The addition of *XaFDH* into the metabolic pathway would help remove excess formate and allow the ADO alkane generation reaction to proceed more efficiently. To explore these possibilities, we used HPLC–UV/MS to measure the relevant metabolites, including NADH, NAD⁺, NADPH, NADP⁺, and formic acid inside the cells and measured the pH change of the system.

Results from measuring NADH, NAD⁺, NADPH, and NADP⁺ using HPLC–UV/MS indicated that the addition of *XaFDH* increased the NADH concentration and the NADH/NAD⁺ redox ratio in *E. coli* cells significantly (Fig. 5A, cell type 4). The *E. coli* strain harboring *XaFDH* (cell type 4) had the highest NADH/NAD⁺ redox ratio, ~1.5-fold higher than the cell type without *XaFDH* after 2 h. The results in Fig. 5A also indicated that the NADH/NAD⁺ redox ratio in *E. coli* cells harboring *XaFDH* (cell types 4 and 5) changed over time, although

Metabolically-engineered pathway for alkane production

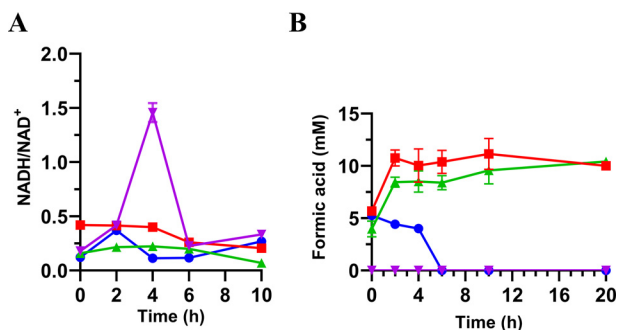


Figure 5. Measurements of related metabolites in the metabolically-engineered cells. *A*, intracellular NADH/NAD⁺ redox ratios; *B*, formate level in whole-cell bioconversion. Native *E. coli* BL21 (DE3) cells (cell type 1) are shown as blue circles; engineered *E. coli* BL21 (DE3) cells harboring the basic pathway for alkane synthesis (cell type 2) are shown as red squares; engineered *E. coli* BL21 (DE3) cells harboring the basic pathway for alkane synthesis with ROS-detoxifying enzymes (TrxA/TrxB) (cell type 3) are shown as green triangles; and engineered *E. coli* BL21 (DE3) cells harboring the basic pathway for alkane synthesis with NADH-regenerating enzyme (*XaFDH*) (cell type 4) are shown as purple triangles. All data are the mean \pm S.D. ($n = 3$).

the ratio in *E. coli* cells without *XaFDH* (cell types 1–3) remained at a similar level throughout the whole period of bioconversion. The NADH/NAD⁺ redox ratio in the *E. coli* strain harboring *XaFDH* decreased after 6 h (Fig. 5A), which is around the same period when tridecane production started to reach the maximum point (Fig. 4B). At this stage, the conversion of tetradecanoic acid to tridecane was less, which in turn also stopped the generation of extra formate, and thus NADH from the *XaFDH* reaction. Despite several attempts, we could only detect cellular NADPH in low amounts, and there was no significant difference in NADPH concentration among the different cell types (data not shown).

It should be noted that the phenomenon of the NADH/NAD⁺ ratio initially increasing and then decreasing in Fig. 5A is not an artifact. These results were also observed when similar experiments using independent setups were performed.⁴ We noted that the NADH/NAD⁺ ratio appeared to be the highest when alkane production reached approximately half of the total yield accumulated.

Results from measuring the formate concentration using HPLC–UV (Fig. 5B) showed that the systems of cell types 2 and 3 have the highest concentrations of formate. Concentrations of formate in the cells expressing *XaFDH* (cell types 4 and 5) are not significantly different from the control cells (cell type 1). These results showed that cells harboring the basic metabolic pathway shown in Scheme 2 accumulated cellular formate concentrations around 10 mM, whereas the pathway including *XaFDH* did not show significant accumulation of formate over the time course of the bioconversion process.

We further explored whether the less efficient production of alkane by the basic metabolic pathway is due to product inhibition of ADO by formate. Activity assays of ADO in the presence of various concentrations of tetradecanal (10–80 μ M) at 10 mM formate or formic acid at a final pH of 7.0 were carried out (Fig. 6). The results clearly showed that ADO activities were the same in the presence or absence of formate/formic acid. These data clearly indicate that formate or formic acid does not inhibit

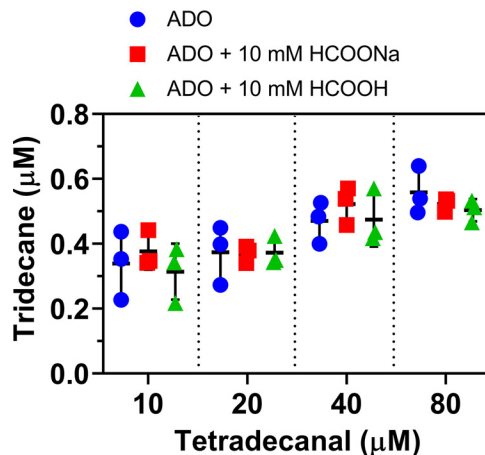


Figure 6. Effect of formic acid and formate to alkane bioproduction. *In vitro* tridecane production by ADO in the presence of 10 mM formate and 10 mM formic acid. Reactions of ADO with various concentrations of tetradecanal (10, 20, 40, and 80 μ M), pH 7.0, were analyzed for the amount of tridecane produced in the presence or absence of formate or formic acid (see “Experimental procedures”). All data represent the mean \pm S.D. ($n = 3$).

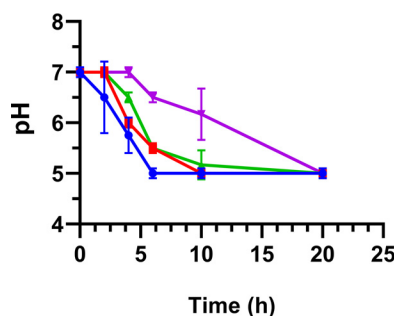


Figure 7. pH profile of cell culture bearing different metabolic pathway constructs. pH values of the metabolically engineered cells after the bioconversion process by native *E. coli* BL21 (DE3) cells (cell type 1) are shown as blue circles; engineered *E. coli* BL21 (DE3) cells harboring basic pathway for alkane synthesis (cell type 2) are shown as red squares; engineered *E. coli* BL21 (DE3) cells harboring the basic pathway for alkane synthesis with ROS-detoxifying enzymes (TrxA/TrxB) (cell type 3) are shown as green triangles; engineered *E. coli* BL21 (DE3) cells harboring the basic pathway for alkane synthesis with NADH-regenerating enzyme (*XaFDH*) (cell type 4) are shown as purple triangles. All data represent the mean \pm S.D. ($n = 3$).

ADO activity and that the improvement of alkane production by addition of *XaFDH* is not due to alleviation of product inhibition.

We then measured the pH of the bioconversion reaction to monitor whether accumulation of formate/formic acid caused pH changes. The results (Fig. 7) indicate that in the absence of *XaFDH*, the pH of the whole-cell bioconversion reactions decreased from the beginning value of 7.5 to pH 5.0 after 6 h. With addition of *XaFDH* in the metabolic path, the pH drop of the reaction was less severe. Cell type 4 that contained *XaFDH* retained a final pH of 6.0–6.5 after 6–10 h of bioconversion. We also assayed the activities of ADO as a function of pH and noted that ADO activity at pH 5.0 was only 44% of the activity at pH 7.0 (Fig. S4). These results imply that by having *XaFDH* co-overexpressed, the cellular pH remained more in the neutral range as compared with the system without *XaFDH*, which keeps ADO more active.

Altogether, the data indicate that the *XaFDH* addition pathway generated more NADH, which may lead to more genera-

⁴ N. Akeratchatapan, unpublished data.

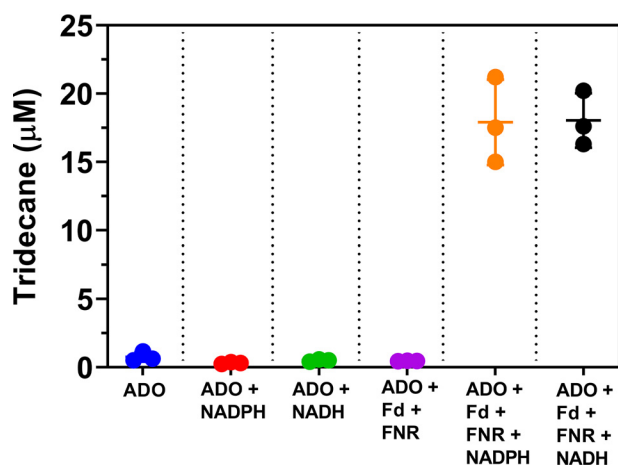


Figure 8. Tridecane production during *in vitro* ADO assays. To demonstrate the reductant effect on ADO activity, the amount of tridecane produced by ADO was measured. Tridecane production by ADO in reactions containing 20 μM ADO; 20 μM ADO and 1 mM NADPH; 20 μM ADO and 1 mM NADH; 20 μM ADO, 40 μM Fd, and 20 μM FNR; 20 μM ADO, 40 μM Fd, 20 μM FNR, and 1 mM NADPH; 20 μM ADO, 40 μM Fd, 20 μM FNR, and 1 mM NADPH are shown in blue, red, green, purple, orange, and black circles, respectively. All enzyme reactions were set up under anaerobic conditions. The reactions were initiated by adding 1 ml of ambient air (21% O_2) and were incubated at 37 $^\circ\text{C}$ for 60 min; the reactions were quenched by adding 1 ml of ethyl acetate containing internal standard (10 μM dodecane and 250 μM tetradecane) and mixed, followed by centrifugation at 18,500 $\times g$ for 10 min to separate the organic phase and analyzed by GC-MS.

tion of alkane. Another factor is that *Xa*FDH can destroy extra formic acid, which also helped maintain the intracellular pH in a range that is more suitable for the engineered metabolic pathway.

Evidence demonstrating the use of NADH by FNR to generate reduced Fd that can be used in alkane production

As the metabolic pathway with *Xa*FDH addition showed a significant level of NADH increase compared with cells with the basic metabolic pathway without FDH (Fig. 5A), these results implied that the increased NADH level might in turn increase the activities of ADO by generating more reduced Fd. Although it was previously reported that the *E. coli* FNR can use NADH as a reductant to catalyze the reduction of cytochrome *c* (39), there was no previous evidence available to demonstrate that FNR can use NADH to generate reduced Fd.

Therefore, we carried out an Fd reduction experiment inside an anaerobic glovebox to identify whether FNR can use NADH as a reductant to generate reduced Fd. A solution of 10 μM FNR in 100 mM HEPES buffer, pH 7.2, containing 100 mM KCl and 100 μM NADH was mixed with 10 μM Fd and 20 μM Fd to monitor the oxidation reaction of NADH for 60 min. The results showed that under the anaerobic conditions employed, the reaction in the presence of FNR, NADH, and purified Fd resulted in NADH oxidation as monitored by the decrease of NADH absorbance at 340 nm (Fig. S5). To detect formation of reduced Fd, which can serve as a substrate for the ADO reaction, the reaction of Fd–NADH–FNR was coupled to the reaction of ADO. Results indicated that the addition of Fd–NADH–FNR to the ADO reaction could result in more tridecane formation compared with the control reactions (Fig. 8), indicating that FNR can use NADH to generate the reduced Fd, which

in turn supports the activity of ADO. In addition, the coupled assay of Fd–NADPH–FNR with ADO was also carried out for comparison. *In vitro* analysis showed that the concentration of tridecane produced from the Fd–NADH–FNR–ADO system is about the same as that produced by the Fd–NADPH–FNR–ADO system (Fig. 8). Although the rate of FNR-catalyzed Fd reduction using NADPH as a reductant is faster than that of NADH (data not shown), the ability of the complete system to produce alkane at similar rates when either NADH or NADPH was used must be due to the slow rate of ADO reaction. Therefore, we have shown for the first time that the FNR–Fd electron transfer system can use NADH to generate reduced Fd and support ADO activity as efficiently as NADPH.

Discussion

Our metabolic pathway reported here demonstrates the system that can produce the highest yield of alkane production from fatty acid reported to date. The key improvement of our system resulted from the addition of *Xa*FDH that can increase the cellular levels of NADH, which in turn generates more reduced Fd for alkane production. The addition of *Xa*FDH also destroys the extra formate accumulated intracellularly that can also maintain the cellular pH in a neutral range.

Alkane biosynthesis in this work utilizes an endogenous pathway of fatty acid uptake and fatty acyl-CoA synthesis in *E. coli* in combination with the engineered pathway containing enzymes for aldehyde synthesis (ACR1) from *A. baumannii* and aldehyde reduction (ADO) from cyanobacteria. Analysis of a starting substrate (fatty acid) and its product (alkane) revealed that the expression of ACR1 and ADO converts fatty acid to alkane in engineered *E. coli* with 35% conversion. Measurements of substrate and product concentrations revealed that fatty acid consumption continued for 20 h while alkane concentrations plateaued at around 6–10 h. The reduced efficiency in alkane biosynthesis observed in *E. coli* over this period was probably caused by a more prominent role of anaerobic fermentation. During the period with low oxygen availability, cellular metabolites such as pyruvate and acetyl-CoA may be accumulated, which can promote the utilization of NADH to produce ethanol and hydroxy acid products such as lactate and acetate (40, 41). Moreover, alcohol synthesis by endogenous aldehyde reductase and alcohol dehydrogenase is another competing pathway for NAD(P)H utilization (42–44). For these reasons, the yield of alkane production by engineered *E. coli* could not reach 100%.

As ADO converts aldehyde into alkane by cleavage of a carbonyl moiety into alkane and formate by-products, accumulation of formate also results in a decrease in pH. The pH of cell type 2, which contained the basic metabolic pathway for alkane production, was measured as pH 5.0 after 6 h.

An improvement of alkane production by our system is derived from the addition of *Xa*FDH into the metabolic pathway. *Xa*FDH used in this work is a new FDH identified to be thermo- and solvent-tolerant and functions well under acidic conditions. *Xa*FDH was expressed to remove formate toxicity by its oxidation to CO_2 with the concomitant gain of an extracellular reductant in the form of NAD(P)H. The increase in the intracellular concentration of NADPH has been shown to be a

Metabolically-engineered pathway for alkane production

major factor enhancing the productivity of NADPH-dependent metabolic pathways (12–14). It was demonstrated that the productivity of terpenoid, an NADPH-dependent terpenoid biosynthesis, was improved by 97% when the pathway was co-expressed with the Entner-Doudoroff operon that can increase the NADPH-generating rate by 25-fold compared with the native strain (14).

In our case, a significant increase of cellular reductant was detected for NADH and not NADPH. The yield of alkane production was significantly higher in cell type 4 in which NADH was much higher than the other cell types. The increase of alkane in the cells containing high levels of NADH might be explained by the ability of NADH to serve as a reductant to generate reduced Fd that can serve as a co-substrate for ADO. The data that demonstrate that NADH can reduce Fd in the reaction of FNR and can be used to generate alkane in the reconstituted system support this conclusion (Fig. 8). Altogether, it can be seen that the increase of cellular NADH can be directly linked to the increase of Fd reduction and, in turn, alkane generation. Another advantage of removal of formic acid accumulation inside the cell is that the system can prolong its pH in the neutral range much better than the system without overexpressed *XaFDH*. The activity of ADO at pH 5.0 was found to be only 45% of the activity at pH 7.0. This result is also similar to the results previously reported in which the activity of ADO decreased upon pH decrease (45). In addition, when the pH of the cell is acidic, it can also affect FNR activity and the production of reduced Fd. It was previously reported that the activity of FNR decreased when the pH was lower (46–48). Studies of the influence of pH on the activity of FNR suggest that high-proton concentration at low pH can perturb the electron transfer from FNR to its electron acceptor by the following: (i) changing the charge moieties of the FNR surface in a way that FNR loses its interaction with its electron acceptor (46, 48), and (ii) modulating the FNR conformation, leading to less efficient binding of substrates (47). Because the generation of reduced Fd is crucial for ADO activity as the reductant for ADO, the acidic pH condition does not support a high-production rate of alkane by ADO.

Our results demonstrated that the addition of an ROS detoxification system does not enhance any yield of alkane production. This result is similar to the results observed in previous studies that co-expression of KatE with ADO enzyme did not promote the production of alkane *in vivo*. This may be because the level of H₂O₂ generated does not accumulate to a very high level. Previous reports showed that the level of H₂O₂ inside *E. coli* cells is typically <1 μM, which might be due to active cellular ROS detoxification systems (49, 50).

In conclusion, the findings here provide a simple but effective approach to enhance alkane production from exogenous fatty acids by the metabolically engineered pathway. The addition of *XaFDH* can convert the formate by-product into valuable NAD(P)H and also prevent a sharp drop of cellular pH due to accumulation of extra formate. This double-pronged approach resulted in a system that gives the highest yield (50%) of bioconversion from fatty acid to alkane to date. This technology should be useful for future applications of converting fat-rich feedstock into biofuel.

Experimental procedures

Materials and methods

All commercially available chemicals were purchased from Sigma, TCI, or Merck. For molecular biology procedures, XL1-Blue competent *E. coli* (Agilent) was used for plasmid amplification, and BL21 (DE3) competent *E. coli* (New England Biolabs) was used for protein overexpression. T4 DNA ligase, restriction enzymes, PCR kits, Gibson kits, and other molecular biology reagents were purchased from New England Biolabs. DNA sequencing was performed by Bioneer (South Korea).

Strain and plasmids

BL21 (DE3) (*fhuA2 (lon) ompT gal (λ DE3) (dcm) ΔhsdS*) cells from Novagen were used for protein expression. The pET17b, pRSFDuet-1, and pCDFduet-1 vectors (Novagen) were used for construction of expression plasmids. Every gene on the Duet-1 vector was controlled by the T7 ribosome-binding site sequence, AAGGAG, of the Duet vector. The preparation of expression plasmids used in this study was described below.

Construction of pET17b-*acr1* plasmid

The *acr1* gene from *A. baumannii* was amplified with the primers ACR1_F and ACR1_R (Table 3) using the genomic DNA of *A. baumannii* as a template. The PCR product was digested with XbaI and XhoI and cloned in a pET17b vector at restriction sites XbaI and XhoI, creating pET17b-*acr1* plasmid.

Construction of pCDF-*fd-fnr-ado* plasmid

For construction of pCDF-*fd-fnr-ado* plasmid, the *ado* gene from *P. marinus* MIT9313 was first cloned into a pCDF-Duet-1 vector. The *ado* gene was amplified with the primers ADO_F and ADO_R (Table 3) using the *ado* gene that was codon-optimized, synthesized, and supplied on pUC57 by Genscript as a template. The PCR product was digested with NdeI and XhoI and cloned into MCS2 of pCDFDuet-1 vector at the restriction sites NdeI and XhoI, creating the pCDF-*ado* plasmid. The pCDF-*ado* was cut with NcoI and EcoRI and ligated into the NcoI/EcoRI-digested PCR product of the *fd* gene from *Synechocystis* sp. PCC 6803, resulting in pCDF-*ado-fd*. Primers Fd_F and Fd_R (Table 3) were used to amplify the *fd* gene that was codon-optimized and synthesized by Genscript. The *fd* gene used in this study encodes 2Fe-2S Fd (51, 52). The *fnr* gene from *E. coli* K-12 was amplified with primers FNR_F and FNR_R (Table 3). The PCR product was digested with EcoRI and PstI and ligated to EcoRI/PstI-digested pCDF-*ado-fd*, yielding the pCDF-*ado-fd-fnr*.

Construction of pRSF-*fdh*, pRSF-*trxA-trxB*, and pRSF-*trxA-trxB-fdh* plasmids

For construction of pRSF-*fdh* plasmid, the *fdh* gene from *Xanthobacter* sp. 91 was amplified with the primers FDH_F and FDH_R (Table 3) using the *fdh* gene that was codon-optimized, synthesized, and supplied on a pUC57 plasmid by Genscript as a template. The resulting PCR product was digested with NdeI and XhoI and ligated with NdeI/XhoI cut pRSFDuet-1 vector to yield the pRSF-*fdh* plasmid. For construction of the pRSF-

Table 3
Primer and gene information used in the engineered metabolic pathway

Gene (ID)	Primers
<i>ado</i> (PMT_1231) ^a	ADO_F: 5'-GCACCATATGCCGACCCTGGAAATG-3' ADO_R: 5'-CCCCTCGAGTTAGCTAACCAGCGCCGCG-3'
<i>acr1</i> (MK492106) ^b	ACR_F: 5'-GCCCTCTAGAAGGAAAATAAAATGAATAAAAAATTAGAAGCTCT-3' ACR_R: 5'-AATATCTCGAGATTACCAATGCTCACCAGG-3'
<i>fd</i> (ssl0020) ^a	Fd_F: 5'-GCACcCATGGCGAGCTACACCGTG-3' Fd_R: 5'-GCCCGGAATTCTTAATACAGGTCCTCTTCc-3'
<i>fnr</i> (b3924) ^a	FNR_F: 5'-GCCCGGAATTCAAGGAGATATACATATGGTGATTGGGTAACAG-3' FNR_R: 5'-CCCCTGCGAGTTACCAGTAATGCTCCGC-3'
<i>Xafdh</i> (WP_029558741.1) ^b	FDH_F: 5'-TATAAGAAGGAGATATACATATGGCGAAGGTGCTGTGC-3' FDH_R: 5'-GCCATATGTATATCTCCTTTTAGCCCGCTTTCTTGAATTTTCG-3'
<i>trxA</i> (PA5240) ^a	trxA_F: 5'-CTTTAATAAGGAGATATACATGAGCGAACATATCGTC-3' trxA_R: 5'-CTCATGGTATATCTCCTTTTCAGATATTGGCGTCGAG-3'
<i>trxB</i> (PA2616) ^a	trxB_F: 5'-CAATATCTGAAAGGAGATATACCATGAGTGAAGTCAAGCATTCG-3' trxB_R: 5'-GGCGCGCCGAGCTCGTCAATGGTCTGCGAGTATTTTTC-3'

^a Information was retrieved from KEGG.^b Information was retrieved from NCBI.

trxA-trxB plasmid, pRSFDuet-1 plasmid was digested with NcoI and XhoI and ligated with the PCR product of *trxA* and *trxB* genes using Gibson assembly kit. The PCR products of *trxA* and *trxB* genes were amplified with primers *trxA_F* and *trxA_R* and primers *trxB_F* and *trxB_R*, respectively, using genomic DNA of *P. aeruginosa* PAO1 as template. For construction of pRSF-*trxA-trxB-fdh* plasmid, pRSFDuet-*fdh* plasmid was digested with NcoI and EcoRI and ligated with the PCR product of *trxA* and *trxB* genes using the Gibson assembly kit.

E. coli whole-cell biocatalyst preparation

The selected gene cassettes in expression plasmids were transformed into competent *E. coli* BL21 (DE3) with 15 ng of each plasmid, and the transformed cells were selected by growing on LB with ampicillin, streptomycin, and kanamycin. A single colony was selected and grown in LB with three antibiotics as a starting liquid culture overnight at 37 °C. The corresponding variant was then subcultured into TB media with 1% inoculant and grown at 37 °C until the OD₆₀₀ reached 0.6. The culture was then induced with 1 mM IPTG and incubated further at 25 °C for 6 h. Bacterial cells were harvested by centrifugation at 4 °C and used for biocatalytic reactions.

Whole-cell biocatalysis and product extraction

The pelleted *E. coli* paste, with expressed proteins, was resuspended and adjusted cell density to OD₆₀₀ of 20 in 100 mM potassium phosphate buffer, pH 7.5, supplemented with 2.5% glucose, and 0.85 mM tetradecanoic acid. The biocatalytic reaction (1 ml) was incubated at 25 °C in a 20-ml gas tight vial for designated periods (0, 2, 4, 6, 10, and 20 h) and quenched by adding 2 ml of ethyl acetate solvent containing internal standards (10 μM dodecane and 250 μM tetradecane) with vigorous mixing. Upon addition of ethyl acetate, the mixture was centrifuged (4 °C, 3900 × g, 20 min) to enhance phase separation, and the upper organic layer was analyzed by GC-MS.

XaFDH expression and purification

The overexpression of the *XaFDH* in *E. coli* BL21 (DE3) was carried out at 25 °C in ZY auto-induction medium system. In

brief, *E. coli* BL21 (DE3) cells harboring pET11a-*Xafdh* plasmid were grown at 37 °C with shaking at 250 rpm to obtain OD₆₀₀ ~1.0, and then the culture was adjusted to a temperature of 25 °C for protein expression. Protein purification was achieved by resuspending cell pellets in 50 mM sodium phosphate buffer, pH 7.0, containing 1 mM DTT, 60 μM PMSF, and 0.5 mM EDTA, disrupting cells by sonication, clearing cell lysates by centrifugation at 28,700 × g at 4 °C for 1 h, and precipitating the protein with 40–60% (w/v) ammonium sulfate. The precipitated proteins were dissolved and dialyzed in 4 liters of 50 mM sodium phosphate buffer, pH 7.0, at 4 °C for 16 h prior to further purification by DEAE-Sepharose anion-exchange chromatography. A linear gradient of 50 mM sodium phosphate buffer, pH 7.0, containing 50–400 mM NaCl was used for protein elution. The fractions of eluted *XaFDH* were pooled and concentrated using stirred cell equipment with a Millipore YM-10 membrane. The purity of *XaFDH* after all steps of purification was analyzed by 12% (w/v) SDS-PAGE.

ADO expression and purification

The overexpression of the ADO was carried out in *E. coli* BL21 (DE3) at 25 °C in ZY auto-induction medium system as mentioned above. *E. coli* BL2 (DE3) harboring pET17b-*ado* plasmid was cultivated for protein expression. The protein purification was achieved by resuspending cell pellets in a lysis buffer (50 mM sodium phosphate buffer, pH 7.0, 1 mM DTT and 100 μM PMSF), disrupting cells by sonication, clearing cell lysates by centrifugation at 28,700 × g at 4 °C for 1 h, removing nucleic acid by using 0.5% (w/v) polyethyleneimine, and precipitating proteins with 40–60% ammonium sulfate. DEAE-Sepharose anion-exchange chromatography was used for further purification. A linear gradient of 50 mM sodium phosphate buffer, pH 7.0, containing 50–250 mM NaCl was used for protein elution. The fractions of eluted ADO were pooled and concentrated, and the buffer was exchanged to 30 mM HEPES buffer, pH 7.0, by using a Sephadex G-25 column. The purity of ADO after all steps of purification was analyzed by 12% (w/v) SDS-PAGE.

Metabolically-engineered pathway for alkane production

Determination of *XaFDH* steady-state kinetics

The steady-state kinetics parameters for *XaFDH* were determined using a spectrophotometric method. In this assay, the K_m and k_{cat} values were determined through initial velocity measurement by varying the concentrations of NAD^+ (0.005–0.800 mM), $NADP^+$ (0.05–40 mM), or formate (5–1000 mM). The *XaFDH* concentration was fixed at 10 nM and 10 μ M when assayed with NAD^+ and $NADP^+$, respectively. The production of NADH and NADPH was monitored by following the UV absorption at 340 nm in 50 mM phosphate buffer at pH 7.0 at 25 °C. The reaction was initiated by adding *XaFDH*. Data were analyzed using the Michaelis-Menten equation to obtain the kinetic parameter k_{cat} and K_m values for all substrates.

Investigation of *XaFDH* stability by ThermoFluor assay

The ThermoFluor assay is a temperature-based assay to determine the stability of proteins using a real-time PCR machine. The assay reaction consisted of 50 mM sodium phosphate buffer, 40 μ M *XaFDH*, and 400 μ M SYPRO Orange dye. The temperature was set from 25 to 90 °C with an increment rate of 1 °C per min. The stability curves and the midpoint values (melting temperature, T_m) were obtained by plotting fluorescence against reaction temperatures. The derivative plot was performed for an easy interpretation of the T_m of protein. The temperature at which the derivative is the lowest point is the T_m .

Investigation of the optimum temperature on *XaFDH*

The optimum temperature of *XaFDH* was investigated by pre-incubating the reaction mixture (50 mM phosphate buffer, pH 7.0, 0.05 mM NAD^+ , 200 mM sodium formate) without enzyme at various temperatures (25, 30, 35, 40, 45, 50, 55, and 60 °C) for 15 min to obtain temperature equilibration. The activity assays were initiated by adding *XaFDH* (2.5 μ M) into the incubated mixture. The absorbance at 340 nm was monitored for NADH production. *XaFDH* activity *versus* temperatures were plotted to examine the optimum temperature of the *XaFDH* reaction.

Investigation of the pH effect on *XaFDH* activity

Activities of *XaFDH* at various pH values were measured at 25 °C in 50 mM sodium phosphate and sodium pyrophosphate buffers for pH ranges of 6–8.5 and 8.5–10, respectively. The assay reactions consisted of 0.05 mM NAD^+ , 200 mM sodium formate, and 2.5 μ M *XaFDH*. The absorbance at 340 nm was monitored for NADH production. Enzyme activities were plotted as a function of final pH values.

Formate inhibition assay

Inhibition of ADO by formate was investigated by measuring initial velocities at various concentrations of tetradecanal (10, 20, 40, and 80 μ M) with a fixed concentration of formate (10 mM) and formic acid (10 mM). The final pH of the reactions was 7.0. The reactions were performed in 100 mM HEPES buffer, pH 7.2, containing 100 mM KCl, 1 μ M ADO, 100 μ M PMS, 1 mM NADH and 40 μ M ferrous ammonium sulfate. Assays were initiated by adding various concentrations of tetradecanal solu-

tion containing 10 mM formate or 10 mM formic acid. The reactions (0.5 ml) were incubated at 37 °C for 1.5 min and quenched by adding 1 ml of ethyl acetate solvent containing internal standards (10 μ M dodecane and 250 μ M tetradecane) with vigorous mixing by a vortex mixer, followed by centrifugation at $18,534 \times g$ for 10 min to separate the organic phase, and analyzed by GC-MS.

Tridecane and tetradecanoic acid analyses

GC-MS using HP5-MS capillary column attached to a mass spectrometer (Agilent 7890B) in electron ionization mode (EI-MS 5977B) was used for analysis of tridecane and tetradecanoic acid. Fragmentation patterns of individual compounds were validated using combined Wiley MS and NIST 2014 databases for known compounds. Quantitative analysis was performed on Agilent ChemStation Quantitative Analysis software to obtain a correlation of known concentrations of each compound *versus* GC-MS signals. The GC condition used was 250 °C at an inlet. Temperature program started at 60 °C for 3 min and ramped to 200 °C with a rate of 10 °C/min, and then stayed at 200 °C for 2 min and ramped to 260 °C at a rate of 20 °C/min, and finally stayed at 260 °C for 3 min. Samples (5 μ l) were used for analysis in each run. Standard curves with known concentrations of standard compounds (1–500 μ M) *versus* GC-MS signals were constructed for analysis of substrate consumed and product formed.

Analysis of cell metabolites

For analyzing formate that was produced during the alkane production process, bioconversion reactions (0.5 ml) were centrifuged for 2 min at $18,500 \times g$ at 4 °C, and the supernatant was then filtered through a 0.2- μ m syringe filter. The resulting filtrate was analyzed by HPLC–UV detection (Agilent) using a cation-exchange column (Agilent Hi-Plex H, 7.7×300 mm, 8 μ m) operated at 50 °C. The analytes were eluted with 0.01 M H_2SO_4 at a flow rate of 0.3 ml/min. The detection wavelength was set at 210 nm. The identity of formate was confirmed by comparison of HPLC profiles with that of the standard formate.

For measuring the intracellular concentration of NADH, NAD^+ , NADPH, and $NAD(P)^+$, bacterial cell pellet was resuspended in 250 μ l of 5 mM ammonium acetate buffer, pH 11, containing 10 μ M L-arabinose as internal standard. The bacterial cells were lysed on ice by sonication. The resulting cell lysate was centrifuged at $18,500 \times g$ at 4 °C for 10 min for separation of supernatant and cell debris. Proteins in the supernatant were removed by Amicon 3-kDa cutoff centrifugal filter device (Millipore). The resulting flow-through was then analyzed by HPLC using ZORBAX SB-Aq RRHD column (2.1-mm inner diameter \times 50 mm, 1.8- μ m particle size). The mobile phase used was 20 mM ammonium acetate buffer, pH 5.0. The flow rate was set to 0.2 ml/min, and the column temperature at 25 °C. The HPLC was directly coupled to HPLC–UV/MS (Agilent 1260 infinity) with an electrospray ionization source operated in a negative ion mode. The mass spectrometer was operated in selected ion monitoring mode to detect and quantify $NAD(P)H$ and $NAD(P)^+$ based on their retention times, UV absorption characteristics, and m/z of the ion. The identities of

NAD(P)H and NAD(P)⁺ were confirmed by comparison with the standard compounds.

In vitro assay of Fd reduction with NADH by FNR

Reduction of Fd with NADH by FNR was assayed in an anaerobic glove box, and the reduction of Fd was measured spectrophotometrically as a decrease in the absorbance of NADH at 340 nm. FNR (10 μ M final concentration) was mixed with Fd (10 and 20 μ M final) and NADH (100 μ M NADH final) in 100 mM HEPES buffer, pH 7.2, containing 100 mM KCl. The reactions were incubated at 25 °C, and the depletion of NADH was monitored at various time points (0, 30, and 60 min).

Activity assay of ADO in the presence of Fd–NADH–FNR and Fd–NADPH–FNR

To compare the efficiency of Fd–NADH–FNR or Fd–NADPH–FNR reducing systems in supporting the activity of ADO, the product of the ADO reaction using Fd–NADH–FNR and Fd–NADPH–FNR as reductants was measured. The enzyme reactions were set up under anaerobic conditions. The reaction contained 20 μ M ADO, 200 μ M tetradecanal, 40 μ M Fd, 20 μ M FNR, and 1 mM NADH or 1 mM NADPH in a total volume of 500 μ l of 100 mM HEPES buffer, pH 7.2, in the presence of 100 mM KCl. Reactions with the same concentrations of ADO, ADO–NADH, ADO–NADPH, and ADO–Fd–FNR were also incubated with 200 μ M tetradecanal in 100 mM HEPES buffer, pH 7.2, in the presence of 100 mM KCl to serve as control reactions. All reactions were initiated by adding 1 ml of ambient air (21% O₂) and were incubated at 37 °C for 60 min and quenched by adding 1 ml of ethyl acetate solvent containing internal standard (10 μ M dodecane and 250 μ M tetradecane). The organic phase was separated by centrifugation at 18,534 \times g for 10 min and subjected to product analysis by GC-MS.

Author contributions—J. J. and P. Chaiyen conceptualization; J. J. and P. I. data curation; J. J., P. I., and P. Chaiyen formal analysis; J. J., T. W., S. M., and R. T. supervision; J. J., P. I., C. K., P. M., P. Chuntaboon, S. B., D. T., and S. M. investigation; J. J., P. I., and C. K. methodology; J. J., P. I., C. K., R. T., and P. Chaiyen writing—original draft; J. J. and P. Chaiyen project administration; P. I. validation; P. Chaiyen funding acquisition; P. Chaiyen writing—review and editing.

References

- Lu, K. (2014) *Materials in Energy Conversion, Harvesting, and Storage*, pp 1–10, John Wiley & Sons, Inc., Hoboken, NJ
- Ho, D. P., Ngo, H. H., and Guo, W. (2014) A minireview on renewable sources for biofuel. *Bioresour. Technol.* **169**, 742–749 [CrossRef Medline](#)
- Lynd, L. R. (2017) The grand challenge of cellulosic biofuels. *Nat. Biotechnol.* **35**, 912–915 [CrossRef Medline](#)
- Hill, J., Nelson, E., Tilman, D., Polasky, S., and Tiffany, D. (2006) Environmental, economic, and energetic costs and benefits of biodiesel and ethanol biofuels. *Proc. Natl. Acad. Sci. U.S.A.* **103**, 11206–11210 [CrossRef Medline](#)
- Peralta-Yahya, P. P., Zhang, F., del Cardayre, S. B., and Keasling, J. D. (2012) Microbial engineering for the production of advanced biofuels. *Nature* **488**, 320–328 [CrossRef Medline](#)
- Lee, S. Y., Kim, H. U., Chae, T. U., Cho, J. S., Kim, J. W., Shin, J. H., Kim, D. I., Ko, Y.-S., Jang, W. D., and Jang, Y.-S. (2019) A comprehensive metabolic map for production of bio-based chemicals. *Nat. Catal.* **2**, 18–33 [CrossRef](#)
- Liao, J. C., Mi, L., Pontrelli, S., and Luo, S. (2016) Fuelling the future: microbial engineering for the production of sustainable biofuels. *Nat. Rev. Microbiol.* **14**, 288–304 [CrossRef Medline](#)
- Zhou, Y. J., Kerkhoven, E. J., and Nielsen, J. (2018) Barriers and opportunities in bio-based production of hydrocarbons. *Nat. Energy* **3**, 925–935 [CrossRef](#)
- Sheil, D. (2009) The impacts and opportunities of oil palm in Southeast Asia: what do we know and what do we need to know? Center for International Forestry Research, Bogor, Indonesia [CrossRef](#)
- Akhtar, M. K., Turner, N. J., and Jones, P. R. (2013) Carboxylic acid reductase is a versatile enzyme for the conversion of fatty acids into fuels and chemical commodities. *Proc. Natl. Acad. Sci. U.S.A.* **110**, 87–92 [CrossRef Medline](#)
- Choi, Y. J., and Lee, S. Y. (2013) Microbial production of short-chain alkanes. *Nature* **502**, 571–574 [CrossRef Medline](#)
- Coursolle, D., Lian, J., Shanklin, J., and Zhao, H. (2015) Production of long chain alcohols and alkanes upon coexpression of an acyl-ACP reductase and aldehyde-deformylating oxygenase with a bacterial type-I fatty acid synthase in *E. coli*. *Mol. Biosyst.* **11**, 2464–2472 [CrossRef Medline](#)
- Harger, M., Zheng, L., Moon, A., Ager, C., An, J. H., Choe, C., Lai, Y. L., Mo, B., Zong, D., Smith, M. D., Egbert, R. G., Mills, J. H., Baker, D., Pultz, I. S., and Siegel, J. B. *et al.* (2013) Expanding the product profile of a microbial alkane biosynthetic pathway. *ACS Synth. Biol.* **2**, 59–62 [CrossRef Medline](#)
- Kallio, P., Pásztor, A., Thiel, K., Akhtar, M. K., and Jones, P. R. (2014) An engineered pathway for the biosynthesis of renewable propane. *Nat. Commun.* **5**, 4731 [CrossRef Medline](#)
- Menon, N., Pásztor, A., Menon, B. R., Kallio, P., Fisher, K., Akhtar, M. K., Leys, D., Jones, P. R., and Scrutton, N. S. (2015) A microbial platform for renewable propane synthesis based on a fermentative butanol pathway. *Biotechnol. Biofuels* **8**, 61 [CrossRef Medline](#)
- Patrikainen, P., Carbonell, V., Thiel, K., Aro, E. M., and Kallio, P. (2017) Comparison of orthologous cyanobacterial aldehyde deformylating oxygenases in the production of volatile C3–C7 alkanes in engineered *E. coli*. *Metab. Eng. Commun.* **5**, 9–18 [CrossRef Medline](#)
- Eser, B. E., Das, D., Han, J., Jones, P. R., and Marsh, E. N. (2011) Oxygen-independent alkane formation by non-heme iron-dependent cyanobacterial aldehyde decarbonylase: investigation of kinetics and requirement for an external electron donor. *Biochemistry* **50**, 10743–10750 [CrossRef Medline](#)
- Khara, B., Menon, N., Levy, C., Mansell, D., Das, D., Marsh, E. N., Leys, D., and Scrutton, N. S. (2013) Production of propane and other short-chain alkanes by structure-based engineering of ligand specificity in aldehyde-deformylating oxygenase. *ChemBiochem* **14**, 1204–1208 [CrossRef Medline](#)
- Andre, C., Kim, S. W., Yu, X. H., and Shanklin, J. (2013) Fusing catalase to an alkane-producing enzyme maintains enzymatic activity by converting the inhibitory by-product H₂O₂ to the cosubstrate O₂. *Proc. Natl. Acad. Sci. U.S.A.* **110**, 3191–3196 [CrossRef Medline](#)
- Bao, L., Li, J. J., Jia, C., Li, M., and Lu, X. (2016) Structure-oriented substrate specificity engineering of aldehyde-deformylating oxygenase towards aldehydes carbon chain length. *Biotechnol. Biofuels* **9**, 185 [CrossRef Medline](#)
- Paul, B., Das, D., Ellington, B., and Marsh, E. N. (2013) Probing the mechanism of cyanobacterial aldehyde decarbonylase using a cyclopropyl aldehyde. *J. Am. Chem. Soc.* **135**, 5234–5237 [CrossRef Medline](#)
- Li, N., Nørgaard, H., Warui, D. M., Booker, S. J., Krebs, C., and Bollinger, J. M., Jr. (2011) Conversion of fatty aldehydes to alka(e)nes and formate by a cyanobacterial aldehyde decarbonylase: cryptic redox by an unusual di-metal oxygenase. *J. Am. Chem. Soc.* **133**, 6158–6161 [CrossRef Medline](#)
- Rajakovich, L. J., Nørgaard, H., Warui, D. M., Chang, W.-C., Li, N., Booker, S. J., Krebs, C., Bollinger, J. M., Jr., and Pandelia, M.-E. (2015) Rapid reduction of the diferric-peroxyhemiacetal intermediate in aldehyde-deformylating oxygenase by a cyanobacterial ferredoxin: evidence for a free-radical mechanism. *J. Am. Chem. Soc.* **137**, 11695–11709 [CrossRef Medline](#)

Metabolically-engineered pathway for alkane production

24. Pandelia, M. E., Li, N., Nørgaard, H., Warui, D. M., Rajakovich, L. J., Chang, W.-C., Booker, S. J., Krebs, C., and Bollinger, J. M., Jr. (2013) Substrate-triggered addition of dioxygen to the diferric cofactor of aldehyde-deformylating oxygenase to form a diferric-peroxide intermediate. *J. Am. Chem. Soc.* **135**, 15801–15812 [CrossRef Medline](#)
25. Warui, D. M., Li, N., Nørgaard, H., Krebs, C., Bollinger, J. M., Jr., and Booker, S. J. (2011) Detection of formate, rather than carbon monoxide, as the stoichiometric coproduct in conversion of fatty aldehydes to alkanes by a cyanobacterial aldehyde decarbonylase. *J. Am. Chem. Soc.* **133**, 3316–3319 [CrossRef Medline](#)
26. Gerlt, J. A., Bouvier, J. T., Davidson, D. B., Imker, H. J., Sadkhin, B., Slater, D. R., and Whalen, K. L. (2015) Enzyme function initiative-enzyme similarity tool (EFI-EST): a web tool for generating protein sequence similarity networks. *Biochim. Biophys. Acta* **1854**, 1019–1037 [CrossRef Medline](#)
27. Wiener, M. C., and Horanyi, P. S. (2011) How hydrophobic molecules traverse the outer membranes of Gram-negative bacteria. *Proc. Natl. Acad. Sci. U.S.A.* **108**, 10929–10930 [CrossRef Medline](#)
28. Chaiyen, P., Suadee, C., and Wilairat, P. (2001) A novel two-protein component flavoprotein hydroxylase. *Eur. J. Biochem.* **268**, 5550–5561 [CrossRef Medline](#)
29. Reiser, S., and Somerville, C. (1997) Isolation of mutants of *Acinetobacter calcoaceticus* deficient in wax ester synthesis and complementation of one mutation with a gene encoding a fatty acyl coenzyme A reductase. *J. Bacteriol.* **179**, 2969–2975 [CrossRef Medline](#)
30. Willis, R. M., Wahlen, B. D., Seefeldt, L. C., and Barney, B. M. (2011) Characterization of a fatty acyl-CoA reductase from *Marinobacter aquaeolei* VT8: a bacterial enzyme catalyzing the reduction of fatty acyl-CoA to fatty alcohol. *Biochemistry* **50**, 10550–10558 [CrossRef Medline](#)
31. Bommarius, A. S., Schwarm, M., Stingl, K., Kottenhahn, M., Huthmacher, K., and Drauz, K. (1995) Synthesis and use of enantiomerically pure *tert*-leucine. *Tetrahedron: Asymmetry* **6**, 2851–2888 [CrossRef](#)
32. Hatrongjit, R., and Packdibamrung, K. (2010) A novel NADP⁺-dependent formate dehydrogenase from *Burkholderia stabilis* 15516: screening, purification and characterization. *Enzyme Microb. Technol.* **46**, 557–561 [CrossRef](#)
33. Tishkov, V. I., Galkin, A. G., Marchenko, G. N., Egorova, O. A., Sheluho, D. V., Kulakova, L. B., Dementieva, L. A., and Egorov, A. M. (1993) Catalytic properties and stability of a *Pseudomonas* sp.101 formate dehydrogenase mutants containing Cys-255–Ser and Cys-255–Met replacements. *Biochem. Biophys. Res. Commun.* **192**, 976–981 [CrossRef Medline](#)
34. Asano, Y., Sekigawa, T., Inukai, H., and Nakazawa, A. (1988) Purification and properties of formate dehydrogenase from *Moraxella* sp. strain C-1. *J. Bacteriol.* **170**, 3189–3193 [CrossRef Medline](#)
35. Galkin, A., Kulakova, L., Tishkov, V., Esaki, N., and Soda, K. (1995) Cloning of formate dehydrogenase gene from a methanol-utilizing bacterium *Mycobacterium vaccae* N10. *Appl. Microbiol. Biotechnol.* **44**, 479–483 [CrossRef Medline](#)
36. Alpdağtas, S., Yücel, S., Kapkaç, H. A., Liu, S., and Binay, B. (2018) Discovery of an acidic, thermostable and highly NADP⁺ dependent formate dehydrogenase from *Lactobacillus buchneri* NRRL B-30929. *Biotechnol. Lett.* **40**, 1135–1147 [CrossRef Medline](#)
37. Mesentsev, A. V., Lamzin, V. S., Tishkov, V. I., Ustinnikova, T. B., and Popov, V. O. (1997) Effect of pH on kinetic parameters of NAD⁺-dependent formate dehydrogenase. *Biochem. J.* **321**, 475–480 [CrossRef Medline](#)
38. Tishkov, V. I., and Popov, V. O. (2004) Catalytic mechanism and application of formate dehydrogenase. *Biochemistry* **69**, 1252–1267 [Medline](#)
39. Leadbeater, C., McIver, L., Campopiano, D. J., Webster, S. P., Baxter, R. L., Kelly, S. M., Price, N. C., Lysek, D. A., Noble, M. A., Chapman, S. K., and Munro, A. W. (2000) Probing the NADPH-binding site of *Escherichia coli* flavodoxin oxidoreductase. *Biochem. J.* **352**, 257–266 [CrossRef Medline](#)
40. Clark, D. P. (1989) The fermentation pathways of *Escherichia coli*. *FEMS Microbiol. Rev.* **5**, 223–234 [CrossRef Medline](#)
41. Unden, G., and Bongaerts, J. (1997) Alternative respiratory pathways of *Escherichia coli*: energetics and transcriptional regulation in response to electron acceptors. *Biochim. Biophys. Acta* **1320**, 217–234 [CrossRef Medline](#)
42. Cao, Y. X., Xiao, W. H., Liu, D., Zhang, J. L., Ding, M. Z., and Yuan, Y. J. (2015) Biosynthesis of odd-chain fatty alcohols in *Escherichia coli*. *Metab. Eng.* **29**, 113–123 [CrossRef Medline](#)
43. Fillet, S., and Adrio, J. L. (2016) Microbial production of fatty alcohols. *World J. Microbiol. Biotechnol.* **32**, 152 [CrossRef Medline](#)
44. Nozzi, N. E., Desai, S. H., Case, A. E., and Atsumi, S. (2014) Metabolic engineering for higher alcohol production. *Metab. Eng.* **25**, 174–182 [CrossRef Medline](#)
45. Waugh, M. W., and Marsh, E. N. (2014) Solvent isotope effects on alkane formation by cyanobacterial aldehyde deformylating oxygenase and their mechanistic implications. *Biochemistry* **53**, 5537–5543 [CrossRef Medline](#)
46. Yeom, J., and Park, W. (2012) Biochemical characterization of ferredoxin-NADP⁺ reductase interaction with flavodoxin in *Pseudomonas putida*. *BMB Rep.* **45**, 476–481 [CrossRef Medline](#)
47. Lee, Y. H., Tamura, K., Maeda, M., Hoshino, M., Sakurai, K., Takahashi, S., Ikegami, T., Hase, T., and Goto, Y. (2007) Cores and pH-dependent dynamics of ferredoxin-NADP⁺ reductase revealed by hydrogen/deuterium exchange. *J. Biol. Chem.* **282**, 5959–5967 [CrossRef Medline](#)
48. Bhatt, A. N., Shukla, N., Aliverti, A., Zanetti, G., and Bhakuni, V. (2005) Modulation of cooperativity in *Mycobacterium tuberculosis* NADPH-ferredoxin reductase: cation- and pH-induced alterations in native conformation and destabilization of the NADP⁺-binding domain. *Protein Sci.* **14**, 980–992 [CrossRef Medline](#)
49. Jang, S., and Imlay, J. A. (2007) Micromolar intracellular hydrogen peroxide disrupts metabolism by damaging iron-sulfur enzymes. *J. Biol. Chem.* **282**, 929–937 [CrossRef Medline](#)
50. Seaver, L. C., and Imlay, J. A. (2004) Are respiratory enzymes the primary sources of intracellular hydrogen peroxide? *J. Biol. Chem.* **279**, 48742–48750 [CrossRef Medline](#)
51. Bottin, H., and Lagoutte, B. (1992) Ferredoxin and flavodoxin from the cyanobacterium *Synechocystis* sp. PCC 6803. *Biochim. Biophys. Acta* **1101**, 48–56 [CrossRef Medline](#)
52. van den Heuvel, R. H., Svergun, D. I., Petoukhov, M. V., Coda, A., Curti, B., Ravasio, S., Vanoni, M. A., and Mattevi, A. (2003) The active conformation of glutamate synthase and its binding to ferredoxin. *J. Mol. Biol.* **330**, 113–128 [CrossRef Medline](#)